



Die Grenzen der
Chemie neu ausloten?
It takes
#HumanChemistry

Wir suchen kreative Chemikerinnen und Chemiker,
die mit uns gemeinsam neue Wege gehen wollen –
mit Fachwissen, Unternehmertum und Kreativität für
innovative Lösungen. Informieren Sie sich unter:

evonik.de/karriere

First-Time Investigations on Cavitation in Rubber Parts Subjected to Constrained Tension Using In Situ Synchrotron X-Ray Microtomography (SR μ CT)

Eric Euchler,* Ricardo Bernhardt, Fabian Wilde, Konrad Schneider, Gert Heinrich, Toshio Tada, Sven Wießner, and Markus Stommel*

Cavitation under constrained tension is a critical failure phenomenon in rubber parts. For laboratory tests, strain constraints can be generated using disk-shaped rubber samples, that is, pancake specimens. Due to suppressed transverse contractibility, the dominating hydrostatic tensile stress, which is the highest in the center part of a pancake specimen, causes an internal failure process controlled by the formation and growth of cavities. Laboratory X-ray microtomography (μ CT) is a powerful tool to monitor the evolution of a cavity population considering various aspects of geometrical as well as microstructural constraints. In the case of carbon black–reinforced styrene-butadiene rubber, microscopic cavities are surrounded by a region of significantly lower material density. Due to detection limits, this region cannot be analyzed in depth with μ CT. In this study, synchrotron X-ray microtomography (SR μ CT) in combination with a modular load frame is used, for the first time, to investigate the damaging phenomenon of cavitation in rubbers. Due to the high phase contrast that can be achieved only by SR μ CT, the microstructure of regions of lower material density can be analyzed and, as a result, tiny satellite cavities are identified in the walls of neighboring microscopic cavities.


of fillers, such as carbon black (CB) or silica. As a consequence, knowledge of the micromechanical deformation and failure behavior is essential for the right choice regarding the compound and the design of technical rubber parts. The first approaches to monitor the deformation-induced structure evolution in rubbers have been performed using advanced imaging techniques, that is, 3D transmission electron microscopy (3D-TEM). Nusser et al.,^[1] Das et al.,^[2,3] and Kadowski et al.^[4] have shown that nano-scale morphological analysis of rubber composites is possible with the help of 3D-TEM. As a result, the knowledge of the evolution of the microstructure of filler-reinforced rubber materials could be improved by information that is barely accessible in 2D methods, for example, the existence of percolated networks^[1] or the presence of individual thin layers of graphene nanoplatelets.^[2,3] Furthermore, results of high-resolution 3D-TEM experiments were used for finite element analysis (FEA) to model the nanostructure between filler aggregates, that is, the glassy bridges.^[4] However, the 3D-TEM technique has some drawbacks: 1) The 3D reconstructions are

Typically, rubbers and rubbery materials are characterized by their macroscopic properties, that is, by the mechanical behavior under external load. However, the macromechanics of rubbers are influenced by the microstructure of the polymer network, for example, the average crosslinking density and the presence

graphene nanoplatelets.^[2,3] Furthermore, results of high-resolution 3D-TEM experiments were used for finite element analysis (FEA) to model the nanostructure between filler aggregates, that is, the glassy bridges.^[4] However, the 3D-TEM technique has some drawbacks: 1) The 3D reconstructions are

E. Euchler, Dr. R. Bernhardt, Dr. K. Schneider, Prof. G. Heinrich, Prof. S. Wießner, Prof. M. Stommel
Institut für Polymerwerkstoffe
Leibniz-Institut für Polymerforschung Dresden e.V.
Hohe Straße 6, 01069 Dresden, Germany
E-mail: euchler-eric@ipfdd.de; stommel@ipfdd.de

Dr. F. Wilde
Institut für Werkstofforschung
Helmholtz-Zentrum Geestacht
Max-Planck-Straße 1, 21502 Geesthacht, Germany

 The ORCID identification number(s) for the author(s) of this article can be found under <https://doi.org/10.1002/adem.202001347>.

© 2021 The Authors. Advanced Engineering Materials published by Wiley-VCH GmbH. This is an open access article under the terms of the Creative Commons Attribution-NonCommercial-NoDerivs License, which permits use and distribution in any medium, provided the original work is properly cited, the use is non-commercial and no modifications or adaptations are made.

DOI: 10.1002/adem.202001347

Prof. G. Heinrich
Institut für Textilmaschinen und Textile Hochleistungswerkstofftechnik
Technische Universität Dresden
Hohe Straße 6, 01069 Dresden, Germany

Dr. T. Tada
Material Research & Development HQ
Sumitomo Rubber Industries Ltd.
2-1-1, Tsutsui-cho, Chuo-ku, Kobe 651-0071, Japan

Prof. M. Stommel
Professur Elastomere Werkstoffe
Institut für Werkstoffwissenschaft
Technische Universität Dresden
Helmholtzstraße 7, 01069 Dresden, Germany

Prof. M. Stommel
Professur Polymerwerkstoffe
Institut für Werkstoffwissenschaft
Technische Universität Dresden
Helmholtzstraße 7, 01069 Dresden, Germany

limited in the capability of detecting individual rubber compound features, such as filler agglomerates or defects, separately due to a limited depth of focus and 2) a rubber sample has to be sufficiently thin, typically in the size of tens of nanometers,^[2,3] to realize the microscopy measurements in transmission mode. The latter aspect is of high importance for in situ experiments to study deformation-induced damage evolution in specimens subjected to geometrical constraints. Such constraints can be generated feasibly only by using samples with sizes in the range of millimeters. A typical deformation-induced damage process is cavitation in rubbers due to a high stress triaxiality, which can be induced by constrained tension using, for example, pancake specimens. Pancake specimens are characterized by a certain diameter-to-thickness ratio, which can be quantified by the shape factor S . If S is high, external loading leads to the formation of an inhomogeneous stress field, where the hydrostatic tensile stress component is dominating in the center of pancake specimens. As a result, the stress triaxiality is high enough to initiate the onset of the internal failure process characterized by the formation and growth of cavities.^[5] Using microscopy techniques, the cavity population can be analyzed on fracture surfaces of pancake specimens *postmortem*.^[6] Further, laboratory X-ray microtomography (μ CT) is a common technique for in situ experiments to obtain local and discretized 3D information of cavities, or other features of the rubber microstructure, for example, filler agglomerates.^[7–9] Typically, μ CT imaging provides a map of variations of X-ray absorption within an object of different structural phases penetrated by the X-ray beam. Depending on experimental factors, for example, the beam energy or the density and effective atomic number of the material, reconstructed μ CT images express the attenuation of each material point within the 3D object. By μ CT scanning, the evolution of cavitation in unfilled and filled rubbers has been investigated by a few research groups.^[7,8,10] In a previous study, the authors of this study performed in situ experiments using a μ CT and a customized load frame to stretch pancake specimens.^[9] As a result, volume strain data obtained by in situ dilatometry experiments could be confirmed via μ CT and, more importantly, extended by discretized imaging data suitable to gather local information and to describe the evolution of the cavity population under tension. **Figure 1** shows the cavitation process of an unfilled styrene-butadiene rubber (SBR) pancake specimen investigated by in situ dilatometry and μ CT experiments.^[9] Thus, the mechanical response, represented by the engineering stress–strain curve (solid line), is extended by volumetric strain data (dashed line) and μ CT slices of the specimens' equatorial plane at elevated strain levels. A scheme of the pancake specimen geometry is shown in the lower right of Figure 1. Resting on the experimental observations, cavitation can be described, generally, by four stages: 1) nearly linear elastic deformation behavior characterized by a remarkable high initial stiffness which is untypical for rubbers; 2) the onset of cavitation, detectable by the increase in volumetric strain leading to stress release due to inelastic damaging resulting in the formation of cavities; 3) the process of cavitation being characterized by a progressive increase in volumetric strain due to the formation of additional cavities and growth of existing ones, where the evolution of cavity morphologies is denoted by the transition from oblate into prolate cavity shapes; 4) the

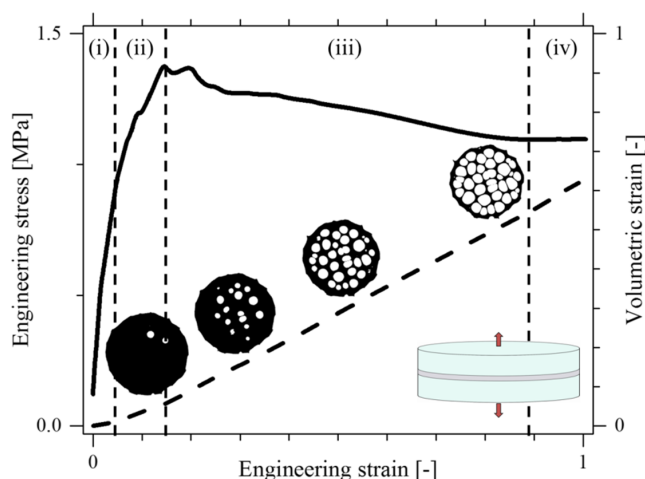


Figure 1. Progress of cavitation in an unfilled SBR pancake specimen characterized by the stress–strain behavior and complementary volumetric strain data as well as corresponding μ CT images. The stages of cavitation (i–iv) are described in the main text. In the lower right, a pancake specimen is shown schematically. The scaling of μ CT slices results from the initial specimen diameter $D = 10.0$ mm.

constraints being fully released and further tensile loading that leads to the deformation of a porous sample until final rupture. Further, as shown in Figure 1, μ CT images of the equatorial plane are suitable to visualize and analyze the reduction of the loaded area of pancake specimens to calculate the true stress values in addition to engineering stress. Due to the high sensitivity of earlier reported in situ dilatometry experiments, the onset of cavitation could be estimated precisely.^[9] Based on the results considering several influencing factors, such as heterogeneity of the crosslinking density or filler content, a cavitation criterion could be defined.^[11] For further information on the influence of the shape factor on the cavitation process, the reader is referred to the Supporting Information or the literature.

Interestingly, cavitation is not restricted to the interfacial failure between rigid filler particles and the soft rubber matrix attributed to inhomogeneous stress fields and local stress concentrations as frequently reported.^[7,8,10] However, in the case of SBR reinforced by a moderate amount of CB, that is, 10–20 parts per hundred rubbers (phr), cavitation is different compared to unfilled SBR. **Figure 2** shows the effects of filler content and strain level on the cavity evolution in SBR investigated by μ CT. Two conclusions can be drawn: 1) The number and size of cavities are increasing with strain and 2) with increasing CB content, the size of cavities is decreasing but their number is increasing. Importantly, in the case of 20 phr CB content, the size of single cavities and the wall thickness between neighboring cavities are close to the spatial resolution limit of μ CT. As a consequence, cavities cannot be characterized as separated objects in the binarized μ CT images for 20 phr CB content. Although in situ experiments give evidence of cavitation due to a remarkable increase in volumetric strain under progressive tension, μ CT seems not to be suitable to detect and separate individual cavities in a similar way to that for unfilled SBR. Likely, there are a lot of very small and closely neighbored cavities that are hard to distinguish by μ CT.

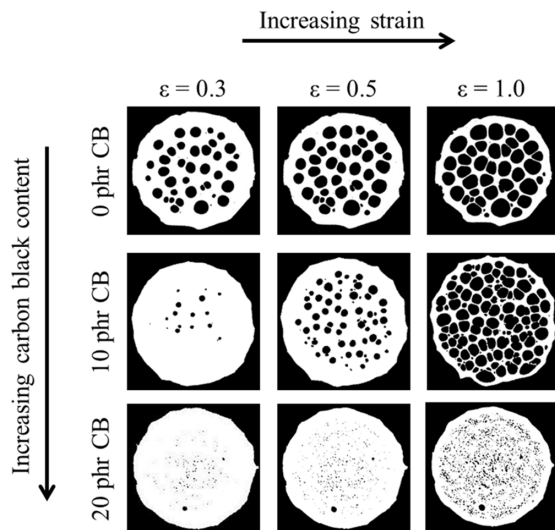


Figure 2. μ CT images showing the cavity evolution under increasing strain, ϵ , for SBR pancake specimens containing different amounts of CB. The scaling results from the initial specimen diameter $D = 10.0$ mm.

The novelty of this study is to conduct synchrotron X-ray microtomography (SR μ CT). Due to the high flux and high brilliance of the monochromatic X-ray beam, the temporal and spatial resolution, as well as the phase contrast, can be improved significantly using synchrotron radiation for tomography or imaging experiments. In comparison to μ CT, the realization of high-resolution SR μ CT scans takes less time by getting comparable effective pixel sizes. More importantly, the phase contrast is of high relevance for this study to distinguish between the material phases *air*, which is within the cavities, and the *rubber matrix*, which has a very low absorption level. Concerning polymer research, the advantages of SR μ CT compared to μ CT have been presented and discussed, for example, by Poulet et al.,^[12] who analyzed the evolution of a defect population in polyamide 11. Although the deformation and failure behavior in semicrystalline thermoplastics, such as polyamide 11, is different compared to that of rubbers, the benefits of the high-phase-contrast SR μ CT measurements have been highlighted. Worth mentioning, in contrast to rubbers, for thermoplastics *crazing* is dominating instead of *cavitation*.

In this study, in situ SR μ CT measurements were performed at the synchrotron facilities of Deutsches Elektronen-Synchrotron (DESY), Hamburg, Germany. The experimental setup of SR μ CT measurements is shown schematically in Figure 3. Rubber pancake specimens were stretched using a customized load frame equipped with a commercially available linear actuator. Force and displacement were logged simultaneously to the metadata of the beamline and were used to obtain the stress–strain characteristics. Because of the specific load frame, the specimen had to be redesigned slightly compared to the specimen geometry used for μ CT. In particular, the initial specimen diameter had to be reduced to allow the beam transmission. Because the diameter-to-thickness ratio has to be high enough, the specimen thickness had to be reduced as well to generate geometrical constraints. For sample imaging, SR μ CT scans were performed at elevated strain levels in propagation-based phase-contrast

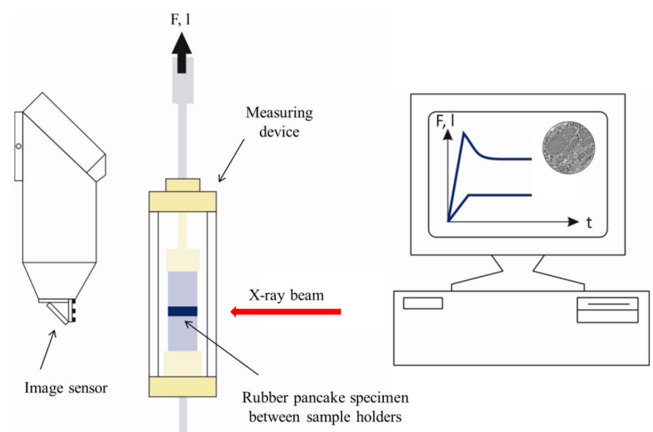


Figure 3. Scheme of the experimental setup for in situ SR μ CT experiments. Technical and methodical information can be found in the main text and the Experimental Section.

tomography. Material degradation needs to be considered when applying high-energy beam measurements, especially in the case of polymer materials. According to Poulet et al.,^[12] who reported that an acquisition time of 90 min is possible without any degradation using a high-intensity beam, degradation was not observed in this study because the acquisition times of the applied experiments were sufficiently low. The reader is referred to the Experimental Section for further information about experimental techniques and methods, for example, data processing and evaluation, as well as on the specifications of the investigated rubber materials.

Figure 4 shows SR μ CT slices of the equatorial plane of an SBR pancake specimen reinforced by 20 phr CB in the unloaded situation and under tension. The obtained SR μ CT slices confirm observations of the previous work,^[9] however, due to the high phase contrast, the cavity population of CB-reinforced rubbers can be characterized in more detail. In Figure 5 new insights on the morphology of a cavity population in SBR reinforced by 20 phr CB are highlighted. The magnifications of the SR μ CT image, which is shown on the right side of Figure 4, show white zones due to the high phase contrast between the *air* within the cavities and the surrounding *rubber matrix*. As a result, different domains in stretched SBR reinforced by 20 phr CB can be distinguished. In detailed views (Figure 5B–D), the specific

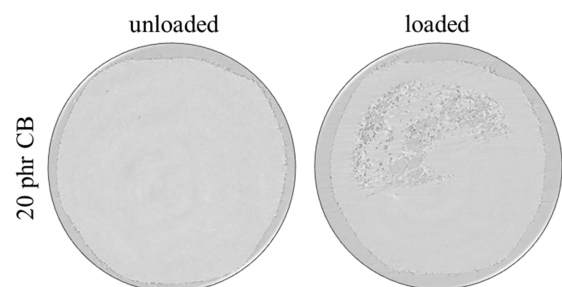


Figure 4. SR μ CT images showing the cavity evolution in a stretched CB-reinforced SBR pancake specimen with a shape factor $S = 5.0$. The scaling results from the initial specimen diameter $D = 5.0$ mm.

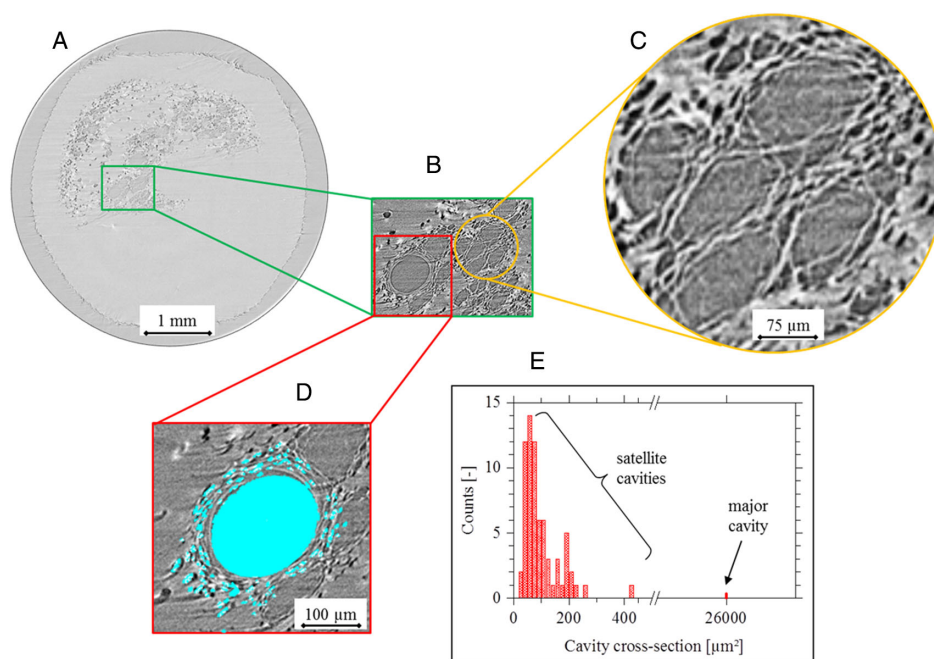


Figure 5. A) SRμCT image of the equatorial plane of an SBR pancake specimen containing 20 phr of CB. B–D) Magnifications of the same SRμCT slice highlighting the phase contrast between single cavities (white lines). E) For the representative material region (D), two types of cavity populations with different magnitudes of the cavity cross-section are expressed by the histogram. A high number of tiny satellite cavities are surrounding the major one.

microstructure of the damaged specimen is highlighted. Here, a significantly high number of tiny satellite cavities can be identified next to major cavities, which are in the size of dozens of microns. As a result, the smallest cavities are reducing the material density locally. In fact, the walls between the larger cavities consist of cavities in the size of a few microns, reducing the effective wall thickness drastically. For a representative material region, the cavity size distribution is quantified by the shown histogram (Figure 5E). To this end, the results of in situ SRμCT give new insights into the mechanisms behind the damaging process due to cavitation observed via in situ μCT. Considering Figure 6, the connection between the results obtained by μCT and SRμCT becomes clear. The dark zones of the nonbinarized, reconstructed μCT image of the slice shown in Figure 2 reveal less dense regions indicating that the center part of the pancake specimens consists of a larger area with a lower material density, but single cavities are barely detectable. Due to the high spatial resolution and phase contrast of SRμCT, a high number of tiny cavities close

to their neighbors were identified, explaining the μCT results. As a result, the damaging process of SBR reinforced by 20 phr CB shows the formation of a third domain—in addition to an undamaged rubber domain and a damaged domain due to cavitation.

Further, the experimental observations shown in Figure 4–6 can be explained considering the network structure of CB-reinforced SBR. In contrast to unfilled materials, filler-reinforced rubbers exhibit a much more complex structure:^[13] 1) the polymer network consisting of chemically crosslinked and entangled polymer chains and 2) filler cluster structures consisting of filler aggregates linked to each other by physical bonds. In the case that a cavity has been formed due to external loading, the cavity growth is mainly controlled by molecular chain scission or failure of crosslinks.^[14] But, because of the presence of the fillers, the cavity growth is suppressed because rigid filler aggregates hinder the progress of chain breakage. Indeed, this micromechanical mechanism is known to be the base of reinforcement in rubbers and other polymers.^[13] However, in terms of cavitation, the presence of a filler network has not been considered to be beneficial for strengthening the rubber resistance against this failure process—at least up to now.

For the first time, in situ SRμCT has been conducted to investigate the fundamental mechanisms behind cavitation in moderately filled rubber materials. While microscopic cavities change their shape from oblate to prolate, tiny satellite cavities will be formed in the walls between microscopic ones. This effect may lead to the local failure of cavity walls, initiating the coalescence of microscopic cavities. The authors suspect an increase of this phenomenon with a further increase of the filler content to a certain—still unknown—limit. Results of other studies^[10,15,16] show that a high amount of reinforcing

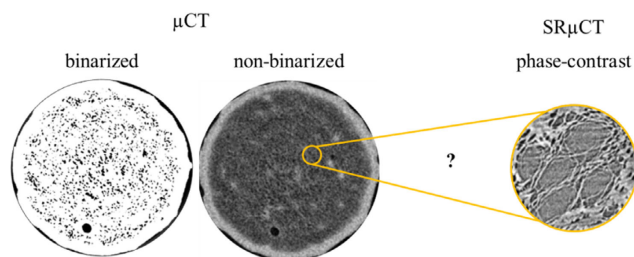


Figure 6. The substructure monitored by SRμCT imaging is suitable to explain the low-density regions within a CB-reinforced SBR observed by μCT scanning.

filler may have a negative effect on the rubber resistance against cavitation due to a dominating interfacial failure between particles and matrix. As a consequence, further investigations studying the impact of different rubber–filler network configurations on cavitation shall be performed in the future. The results of this study have shown that in situ propagation-based phase-contrast SR μ CT scanning is a powerful tool; however, such experiments are limited to synchrotron radiation. In addition to high phase contrast, high-resolution in situ experiments are required to investigate the initial steps of cavity nucleation, which was not possible by the SR μ CT method used in this study. Next, quantitative data analysis, for example, in terms of characterizing changes in cavity shapes and cavity volume fraction, will be intensified by subsequent measurements. Further investigations are required because the spatial resolution of the used SR μ CT method did not allow for describing the initial step of cavity initiation. Probably, rapid or “on-the-fly” scanning will be expedient to study the transition from initiation to failure due to cavity growth. Finally, a goal of further studies is to achieve appropriate experimental data describing the deformation and failure mechanisms on the microscale for different rubber materials to develop and provide relevant constitutive models for finite element methods.

Experimental Section

Materials: The investigated rubber compounds consisted of the following ingredients: 100.0 phr SBR Nipol 1502 (Zeon Co., Japan), 0–20.0 phr CB N220, 2.0 phr stearic acid, 2.0 phr antioxidants, 1.4 phr sulfur, and 1.3 phr accelerator. The processing was realized by Sumitomo Rubber Industries Ltd., Japan, using an internal mixer. The green rubber was vulcanized to thin rubber sheets in a heat press at 170 °C according to rheometric measurements using a Rubber Process Analyzer from TA Instruments, US.

Specimens: Pancake specimens were produced by gluing thin, disk-shaped rubber sheets between cylindrical polycarbonate sample holders. The geometrical constraints of pancake specimens can be quantified by the shape factor S characterizing the diameter-to-thickness relation, where D and h are the initial value of the diameter and thickness, respectively.^[6]

$$S = \frac{D}{4h} \quad (1)$$

For μ CT experiments, the specimens were characterized by $D = 10$ mm and $h = 0.50$ mm, for SR μ CT, specimens with $D = 5$ mm and $h = 0.25$ mm were used. The failure behavior is not affected by the single values of D and h , but only by its relation S .^[6,9] Due to the small specimen volume, the whole specimen could be inspected by one single μ CT or SR μ CT scan even at high strain levels.

For mounting the delicate specimens into the load frames, shape distortion needs to be prevented avoiding any predamage of the rubber. All tensile tests were performed under quasistatic tension at ambient conditions. The reproducibility of the deformation and failure behavior was checked by repeating the experiments at least twice. To better understand the mechanisms behind cavitation, the reader is referred to Figure S1, Supporting Information, highlighting the influence of the shape factor on the deformation and failure behavior of rubbers.

In Situ μ CT: A vivaCT75 scanner from SCANCO Medical, Switzerland, was used for in situ μ CT measurements in absorption. For stretching the pancake specimens, a customized loading device was used, which is described in detail in a previous study by the authors.^[9] Briefly, the pancake specimens were fixed in a polycarbonate tubular load frame with an outer and inner diameter of 30 and 15 mm, respectively. A load sensor measured continuously the force during stepwise loading applied by an

electromechanical actuator. Because stress relaxation could blur μ CT images, a relaxation time of 2 min was considered after each loading step before performing the μ CT scans. Reconstruction, thresholding, and filtering were done with the help of SCANCO Medical evaluation software. Further data analysis was realized using the open-source software tools from ImageJ. For in situ μ CT experiments, the spatial resolution was limited to an effective voxel size of $(10 \mu\text{m})^3$.

In Situ SR μ CT: In situ SR μ CT experiments were performed at the PETRA III Imaging Beamline P05, Deutsches Elektronen-Synchrotron (DESY), Hamburg, Germany, operated by Helmholtz-Zentrum Geesthacht (HZG).^[17] A monochromatic beam was provided by a double multilayer monochromator at 30 keV. Transmitted X-rays were detected by a high-sensitivity pipelined global shutter CMOS image sensor, type CMV20000 from ams AG, Austria. The sensor resolution was 5120×3840 pixels with a pixel size of $6.4 \mu\text{m}$. One SR μ CT scan of 360° with a step width of 0.15° took ≈ 20 min. The optical magnification of $20\times$ and the beam profile allowed a field of view (FoV) of 7.33 mm^2 . For the propagation phase contrast, a sample-to-detector distance of 60 mm was set to allow a good combination of absorption and phase contrast. Similar to μ CT measurements, the pancake specimens were fixed in a polymethylmethacrylate tubular load frame with an outer and inner diameter of 50 and 28 mm, respectively. The specimens were placed vertically within the load frame and centered on the rotation axis. SR μ CT scanning was realized at once at several loading steps while the mechanical properties, force and displacement, were recorded simultaneously. The stepwise loading was applied using an electromechanical actuator, type MA-35 from Physik Instrumente (PI) GmbH & Co. KG, Germany. In-depth information about the load frame that was used for the in situ SR μ CT experiments can be found in the literature.^[18] Again, a relaxation time of 2 min was considered after each loading step before performing the SR μ CT scans. After the acquisition, the reconstruction of the SR μ CT data was done with the help of beamline-provided reconstruction routines utilizing Matlab scripts based on the ASTRA toolkit.^[19,20] Further data analysis was realized using the open-source software tools from ImageJ, but due to the phase-contrast mode of the SR μ CT scanning, quantitative analysis of the obtained data was barely possible, at least not in an automated manner. For the SR μ CT experiments of this study, the effective voxel size was $(2.5 \mu\text{m})^3$.

Supporting Information

Supporting Information is available from the Wiley Online Library or from the author.

Acknowledgements

The authors thank Sumitomo Rubber Industries Ltd., Japan, for the generous financial support.

Open access funding enabled and organized by Projekt DEAL.

Conflict of Interest

The authors declare no conflict of interest.

Data Availability Statement

Research data are not shared.

Keywords

cavitation, phase-contrast tomography, rubbers, strain constraints, X-ray imaging

Received: November 10, 2020

Revised: February 25, 2021

Published online: March 19, 2021

- [1] K. Nusser, T. Mosbauer, G. J. Schneider, K. Brandt, G. Weidemann, J. Goebbels, H. Riesemeier, D. Göritz, *J. Non-Cryst. Solids* **2012**, 358, 557.
- [2] A. Das, R. Boldt, R. Jurk, D. Jehnichen, D. Fischer, K. W. Stöckelhuber, G. Heinrich, *RSC Adv.* **2014**, 4, 9300.
- [3] A. Das, R. Boldt, R. Jurk, D. Jehnichen, D. Fischer, K. W. Stöckelhuber, G. Heinrich, *RSC Adv.* **2014**, 4, 58083.
- [4] H. Kadowaki, G. Hashimoto, H. Okuda, T. Higuchi, H. Jinnai, E. Seta, T. Saguchi, *Mech. Eng. J.* **2016**, 3, 16.
- [5] A. N. Gent, P. B. Lindley, *Nature* **1957**, 180, 912.
- [6] N. A. Hocine, A. Hamdi, M. Naït Abdelaziz, P. Heuillet, F. Zaïri, *Int. J. Solids Struct.* **2011**, 48, 1248.
- [7] E. Bayraktar, S. Antolovich, C. Bathias, *Int. J. Fatigue* **2006**, 28, 1322.
- [8] K. Le Gorju Jago, *Rubber Chem. Technol.* **2012**, 85, 387.
- [9] E. Euchler, R. Bernhardt, K. Schneider, G. Heinrich, S. Wießner, T. Tada, *Polymer* **2020**, 187, 122086.
- [10] B. Huneau, I. Masquelier, Y. Marco, V. Le Saux, S. Noizet, C. Schiel, P. Charrier, *Rubber Chem. Technol.* **2016**, 89, 126.
- [11] E. Euchler, R. Bernhardt, K. Schneider, G. Heinrich, T. Tada, S. Wießner, M. Stommel, in *Advances in Polymer Science* (Eds.: R. Stocck, G. Heinrich, R. Kipscholl), Springer, Berlin **2020**.
- [12] P.-A. Poulet, G. Hochstetter, A. King, H. Proudhon, S. Joannès, L. Laiarinandrasana, *Polym. Test.* **2016**, 56, 245.
- [13] T. A. Vilgis, G. Heinrich, M. Klüppel, *Reinforcement of Polymer Nano-Composites: Theory, Experiments and Applications*, Cambridge University Press, Cambridge **2009**.
- [14] M. Stratigaki, C. Baumann, L. C. A. van Breemen, J. P. A. Heuts, R. P. Sijbesma, R. Göstl, *Polym. Chem.* **2020**, 11, 358.
- [15] T. Shinomura, M. Takahashi, *Rubber Chem. Technol.* **1970**, 43, 1025.
- [16] T. Goudarzi, D. W. Spring, G. H. Paulino, O. Lopez-Pamies, *J. Mech. Phys. Solids* **2015**, 80, 37.
- [17] F. Wilde, M. Ogurreck, I. Grevig, J. U. Hammel, F. Beckmann, A. Hipp, L. Lottermoser, I. Khokhriakov, P. Lytaev, T. Dose, H. Burmester, M. Müller, A. Schreyer, *AIP Conf. Proc.* **2016**, 1741, 030035.
- [18] J. Moosmann, D. C. F. Wieland, B. Zeller-Plumhoff, S. Galli, D. Krüger, A. Ershov, S. Lautner, J. Sartori, M. Dean, S. Köhring, H. Burmester, T. Dose, N. Peruzzi, A. Wennerberg, R. Willumeit-Römer, F. Wilde, P. Heuser, J. U. Hammel, F. Beckmann, in *Proc. SPIE*, Vol. 11113, SPIE, San Diego, CA, USA **2019**.
- [19] J. Moosmann, A. Ershov, V. Weinhardt, T. Baumbach, M. S. Prasad, C. LaBonne, X. Xiao, J. Kashef, R. Hofmann, *Nat. Protoc.* **2014**, 9, 294.
- [20] W. van Aarle, W. J. Palenstijn, J. De Beenhouwer, T. Altantzis, S. Bals, K. J. Batenburg, J. Sijbers, *Ultramicroscopy* **2015**, 157, 35.